

Geochemical and Lithological Controls on a Potential Shale Reservoir: Carboniferous Holywell Shale, Wales

Leo P. Newport ^{a*}, Andrew C. Aplin ^a, Jon G. Gluyas ^a, H. Chris Greenwell ^a,
Darren R. Gröcke ^a

^a*Durham University, Department of Earth Sciences, Science Labs, Durham, DH1 3LE, UK*

* *Corresponding authors. Email address: leo.newport@durham.ac.uk*

Abstract

The Holywell Shale is part of the Carboniferous Bowland Shale Formation, identified as the main potential shale gas system in the UK. Here, we report geochemical and petrographic data from five outcrops of the Lower and Upper Holywell Shale across northeast Wales. At outcrop, the Holywell Shale is immature to early oil mature and has total organic carbon (TOC) values ranging between 0.1 to 10.3 wt. %, with a mean of 1.9 wt.%. Carbon isotope data clearly differentiate terrestrial and marine organic matter and show that both occur throughout the Holywell, with terrestrial sources (Type III/IV) dominating the Upper Holywell and marine sources dominating the Lower Holywell (Type II/III). Trace element data indicate that bottom waters were oxygenated, resulting in poorly preserved organic matter, supported by C/N and HI data. A range of silt- and clay-rich lithofacies occur, which show no relationship to either the amount or type of organic matter. We interpret the data in terms of a mixed supply of terrestrial and marine organic matter to marine depositional environments in which there was sufficient hydrodynamic energy to transport fine-grained sediment as bed load. The resulting mudstones exhibit a range of sedimentary textures with millimetre- to centimetre-scale silt-clay bed forms which show almost no relationship to organic matter type and amount. The small-scale variability and heterogeneity of both organofacies and lithofacies means that the reservoir quality of the Holywell Shale is inherently difficult to predict.

Keywords: Bowland Shale; mudstone; source rock; shale gas; lithofacies; organofacies; Carboniferous; petrography.

1. Introduction

Over the past decade the production of hydrocarbons from unconventional sources has increased significantly, specifically with the development and exploitation of mudstone source-rock reservoirs where hydrocarbons have been generated *in-situ* (Hart et al., 2013). A key shale gas target in the UK is the Carboniferous Bowland-Hodder Formation of the Pennine Basin (Andrews, 2013). The present study focuses on the Holywell Shale deposits of northeast Wales, part of the Bowland Shale Formation, and investigates the way in which a complex interplay of sediment supply, depositional environment and provenance and preservation of organic matter influences the source-rock reservoir quality of this major mudstone unit.

The Carboniferous basins of northern England, including the Pennine Basin in which the Holywell Shale was deposited (Figure 1), were formed during the Dinantian (359.2–326.4 Ma) by a phase of rifting that was dominated by N-S extension acting along pre-existing NW-SE and NE-SW post-Caledonian weaknesses to create asymmetrical half-graben structures. Subsequent Namurian sedimentation (326.4–314.5 Ma) occurred during a period of post-rift thermal subsidence which created sufficient accommodation space for the accumulation of up to 2 km of sediments, including the Holywell Shale (Fraser & Gawthorpe, 1990; Williams & Eaton, 1993). The type-section for the Holywell Shale is contained within the Abbey Mills borehole with a maximum thickness of 152m (Davies et al., 2004; Waters, 2009).

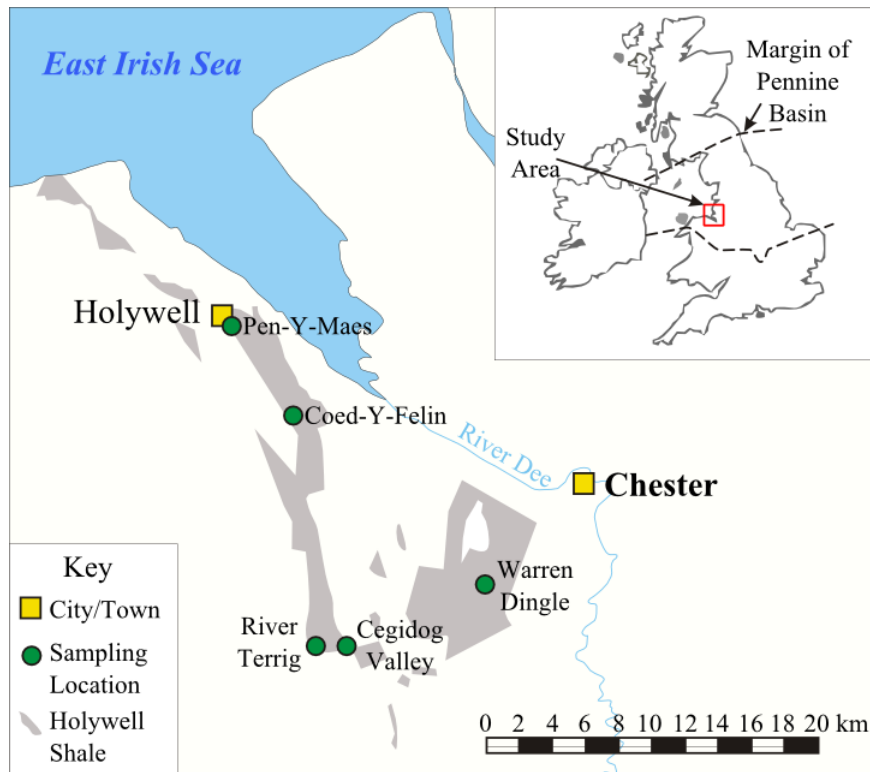


Figure 1: Map of the study area with the wider location (inset image), showing the extent of the Holywell Shale (grey) and the main outcrop locations studied.

Namurian sedimentation in northern England generally occurred in a shallow epicontinental seaway within a series of connected basins stretching across the UK and Ireland (Figure 2; Davies et al., 1999). Sediment was supplied from the north into deltaic systems and shallow seas and deposited in water depths of less than 100-200 m (Figure 2; Wells et al., 2005). Sea levels in the late Mississippian and early Pennsylvanian were also strongly influenced by a series of glacioeustatic cycles which resulted in global sea level variations of 60-100 m (Rygel et al., 2008) which are well recognised in the UK Namurian (Armstrong et al., 1997; Bott & Johnson, 1967; Church & Gawthorpe, 1994; Hampson et al., 1996; Jerrett & Hampson, 2007; Martinsen et al., 1995; Ramsbottom, 1977; Wright et al., 1927). The Holywell Shale was thus deposited as a succession of marine, brackish and non-marine mudstones on the southwest edge of the Pennine Basin (Figure 2; Collinson, 1988; Davies et al., 2004; Guion & Fielding, 1988). Maximum flooding surfaces are represented by a series of ammonoid (goniatite) marine bands

up to several metres thick, which contain assemblages of both benthic and planktonic fauna and which represent a range of fresh water to saline environments (Waters et al., 2009). These marine bands allow the Holywell Shale to be dated biostratigraphically (Figure 3; Davies et al., 2004; Ramsbottom, 1974; Ramsbottom et al., 1978; Waters & Condon, 2012).

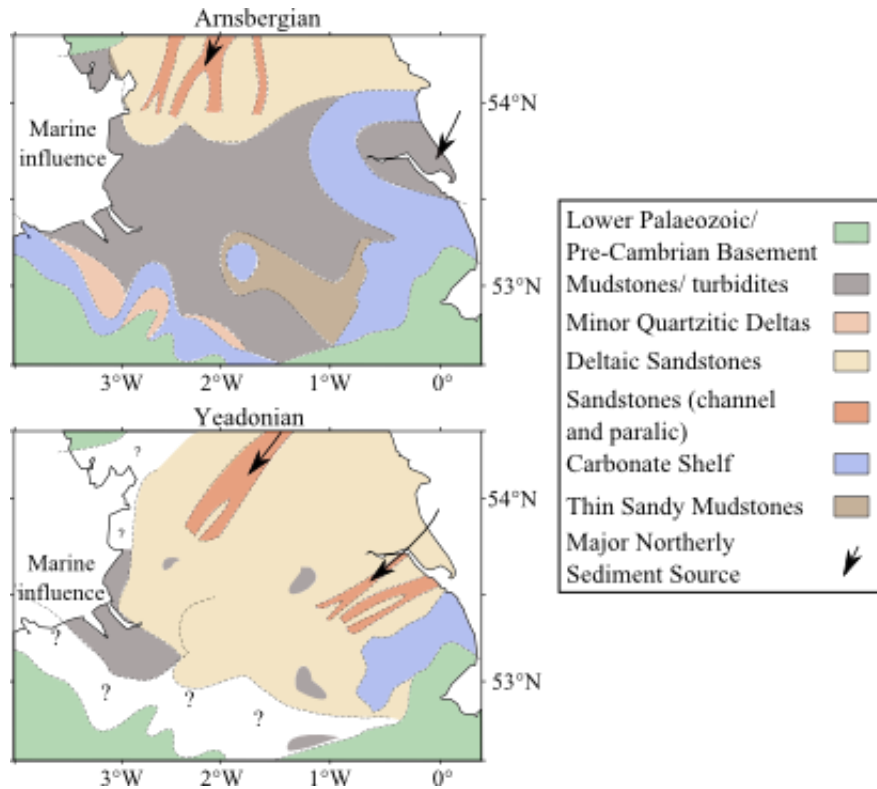


Figure 2: Palaeogeography of the Arnsbergian (top) and Yeadonian (bottom) showing the progradation of the major northerly sourced delta systems (adapted from Fraser & Gawthorpe, 2003).

Organic carbon contents of Namurian mud-rich sediments in northern England typically range from 1–3%, with values up to 8% (Andrews, 2013). Palynological and carbon isotope studies show that the organic matter is derived from both marine and terrestrial sources (Stephenson et al., 2008; Davies et al., 2012). Previous work suggests that at least parts of the Lower Holywell Shale (E1c age; Figure 3) has petroleum potential and may have sourced oils in the Douglas and Lennox oilfields in the East Irish Sea (Armstrong et al., 1997).

The quality of shale reservoirs relates to both their gas/oil storage potential and the rate at which that petroleum can be delivered to a wellbore from matrix pores to a fracture network induced by hydraulic fracturing. These factors relate in turn to the nature and amount of organic matter in the rocks, and also their lithology and mineralogy (e.g. Passey et al., 2010). In a depositional system like the Holywell Shale, in which both water depth and the supply of both sediment and organic matter changed over short periods of geological time, controls on shale reservoir quality will be complex in both space and time, and thus difficult to predict. In this context, we look here at a series of samples from both the Lower (Pendleian to Arnsbergian) and Upper (Marsdenian to Yeadonian) units of the Holywell Shale to determine whether there are relationships between the sedimentology and mineralogy of the rocks and the nature and amount of organic matter.

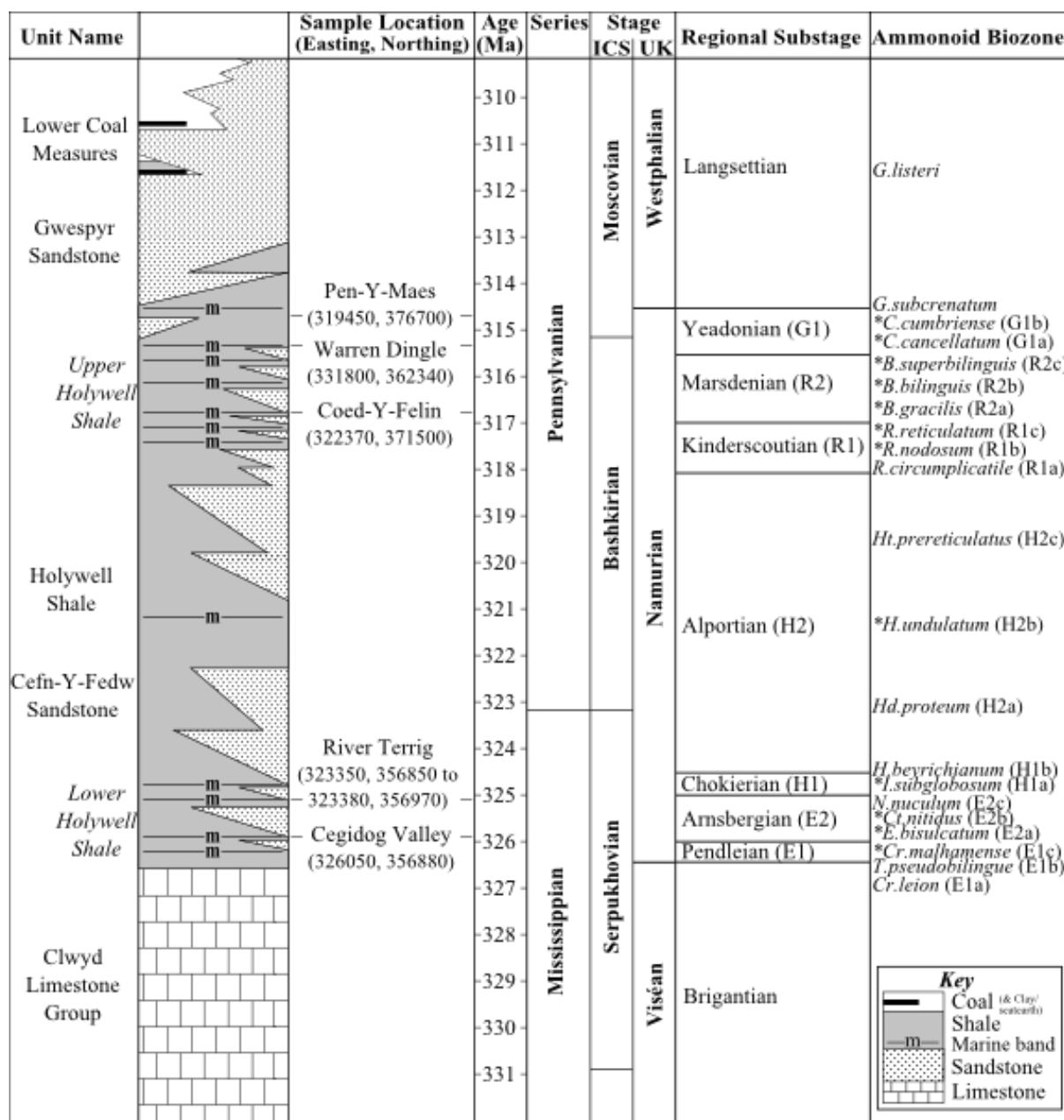


Figure 3: A simplified stratigraphic column of the Holywell Shale, Gwespyr and Cefn-Y-Fedw Sandstone units; Westphalian Lower Coal Measures; Viséan Limestones. Sample locations and their ages relative to Namurian regional chronostratigraphy and biostratigraphy (* denotes ammonoid biozone recorded within the Holywell Shale in the northeast Wales region) (adapted from Davies et al., 2004; Jerrett & Hampson, 2007; Jones & Lloyd, 1942; Waters & Condon, 2012).

2. Methods

2.1: Sample Site Description

Samples were collected from outcrops of the Holywell Shale. Outcrop access was restricted due to the limited exposure of the Holywell Shale within northeast Wales (Figure 1). The outcrops sampled consisted of narrow sections (< 1 m) within stream cuttings, where samples were taken from an area of ~ 0.5 m². In the case of River Terrig and Pen-Y-Maes, which were more extensive, multiple sites were sampled along the exposures and therefore, represent a more significant range in stratigraphy (Figure 3). Due to faulting, the River Terrig location does not represent a continuous sequence of deposition and the stratigraphic placement of this location is difficult as the E2b3 pelagic goniatite fauna (*Cravenoceratoides nititoides*) is only reported as present on the north side of the fault (RTS2 sampling site, with RTS3, RTS5, RTS6 sampling sites occurring close to the faulted zone) (Waters & Condon, 2011). It is not clear from outcrop analysis what type of faulting has occurred, it has been assumed that the fault is normal with the north side of the fault (with the fossil marine band present) downthrown therefore representing younger material than the southern side (RTS1 sample site) of the fault.

2.2: Sample Collection and Analysis

At each sampling location (Figures 1 & 3) samples were collected at random across the available exposure from base to top. Weathered material was removed until a fresh surface of mudstone was accessible: in some cases this resulted in over 20 cm of material being removed. All samples were dried at room temperature, powdered using an agate mortar and pestle and subsequently re-dried in an oven at 40 °C. Polished thin sections of select samples were created by cutting the shale sample into 1 cm thick slices and mounting them to glass slides using an epoxy resin (Epo Tek 301) and polishing to 15 µm for optical thin sections and 50 µm for SEM thin sections.

Total organic carbon (TOC), total nitrogen (TN) & stable isotope analysis

Sample preparation involved weighing the mass of the sample followed by a treatment of 3 M hydrochloric acid that de-calcified the powdered samples. Samples were then rinsed with de-ionised water until neutrality was obtained, subsequently dried in an oven at 60 °C, and after drying the samples required re-powdering. Total organic carbon, total nitrogen content and stable isotope analysis of the samples were performed using a Costech Elemental Analyser (ECS 4010) connected to a ThermoFinnigan Delta V Advantage isotope ratio mass spectrometer. Carbon isotope ratios were corrected for ^{17}O contribution and reported in the standard delta (δ) notation in per mil (‰) relative to Vienna Pee Dee Belemnite (VPDB). Isotopic accuracy was monitored through routine analyses of in-house standards, which were stringently calibrated against international standards (e.g., USGS 40, USGS 24, IAEA 600, IAEA N1, IAEA N2): this provided a linear range in $\delta^{13}\text{C}$ between -46.7 ‰ and $+2.9$ ‰ and in $\delta^{15}\text{N}$ between -4.5 ‰ and $+20.4$ ‰. Analytical uncertainty in carbon isotope analysis was typically ± 0.1 ‰ for replicate analyses of the international standards and typically < 0.2 ‰ on replicate sample analysis. Analytical uncertainty in nitrogen isotope analysis was typically ± 0.1 ‰ for replicate analyses of the international standards and typically < 0.2 ‰ on replicate sample analysis. Total organic carbon data was obtained as part of the isotopic analysis using gas chromatography in the Costech Elemental Analyser (ECS 4010) where the quantity of elemental CO_2 were measured against an internal standard (Glutamic Acid, 40.82 % C) on a thermal conductivity detector (TCD). Nitrogen isotope analysis was performed separately to the carbon isotope analysis. A carbon dioxide (CO_2) trap was installed in the Costech Elemental Analyser so that only N_2 gas entered the isotope ratio mass spectrometer, and nitrogen isotope ratios with a signal strength over 1000 mV are only reported in this study. Total nitrogen data was obtained as part of the isotopic analysis in the same way as total carbon using gas chromatography and measuring elemental N_2 against an internal standard (Glutamic Acid, 9.52

% N) on a TCD. Results were corrected for the calcite lost as a result of acidification and represent %N on the original samples.

Kerogen Type & Maturity

RockEval™ analysis of the outcrop samples was completed using a RockEval™ II analyser. RockEval™ is a pyrolysis based technique which determines the type and maturity of organic matter and thus its petroleum generation potential (Espitalié et al., 1977). Between 50–100 mg of powdered whole rock samples were pyrolysed in an inert Helium atmosphere from 180 °C to 600 °C, using a ramp rate of 25 °C per minute. The mass of hydrocarbon vapours produced at 300 °C (free hydrocarbons) was analysed using a flame ionising detector (FID), to give the S₁ peak of the pyrogram. The temperature was then increased from 300 °C to 550 °C in order to crack non-volatile organic matter, i.e. kerogen. The vaporised hydrocarbons measured by the FID during this heating phase represent the S₂ peak on the pyrogram. The temperature at which the S₂ peak reaches maximum generation is termed the T_{max}. Further parameters were derived using the following equations (Tissot & Welte, 1984): (i) hydrogen index; HI = (S₂/TOC)x100; (ii) production index; PI = S₁/(S₁+S₂); (iii) transformation index; TI = S₁/TOC; and (iv) pyrolysate yield; PY = S₁+S₂.

Analysis of Mineral Phases

X-ray diffraction (XRD) analysis of the outcrop samples was undertaken using a Bruker D8 Advance (D8000 diffractometer), with a wavelength of 1.5406 nm (Cu K_{α1} radiation). The machine was calibrated using Al₂O₃, Y₂O₃, and SiO₂ standards. Bulk powder samples were continuously rotated and scanned from 5-90 ° (2θ), with measurements taken every 0.02 ° (2θ). Total scan time was 1256 seconds (20 minutes 56 seconds) with a time per step of 3.146 seconds. The clay fraction was not separated for further analysis in this study.

X-Ray Fluorescence spectroscopy

X-ray fluorescence (XRF) spectroscopy analysis of the outcrop samples was conducted using a SPECTRO XEPOS ED-XRF. Powdered samples (~ 4 g) were pressed into 30 mm diameter pellets. Major, minor and trace elements were measured using a solid state lithium-drifted silicon detector (Si (Li)). Analytical uncertainty was typically < 1 % relative standard deviation.

Optical Thin Section Analysis

Samples were scanned using a HP Deskjet F4200 series flatbed scanner to show visible variations in colour and structures. Scan settings used were: 2400 DPI, no magnification was used. Textures in the thin sections were studied using a Leica DM 1B02 petrographic microscope, and images were captured using the attached digital camera (Leica DFC 320).

Scanning Electron Microscopy (SEM)

Thin sections of selected outcrop samples were carbon coated (15 nm) and examined using a Hitachi SU-70 High Resolution Analytical SEM, equipped with an Oxford Instrument Energy Dispersive X-ray (EDX) and microanalysis system (INCA Energy 700). SEM imaging, both secondary electron (SE) and back scattered electron (BSE) modes, was used to investigate the mineralogy and texture (including: mineral/grain roundness, sphericity, size, distribution and etching/scratching to the surface of grains) of the samples. BSE mode allowed mineral phases to be differentiated according to atomic number. For selected areas, EDX was used to create mineral maps based on elemental distribution.

3. Results

3.1: Organic Geochemistry

The average TOC across the Holywell Shale in this study is 1.9 wt % with both the highest (10.3 wt %) and lowest (0.1 wt %) values recorded within the Upper Holywell Shale (Table 1). The range of TOC within the Lower Holywell Shale is 0.6 wt % to 3.4 wt % with an average

of 2.0 wt %. RockEval™ data show that the organic matter ranges from mixed Type II/III to Type III/IV and that the samples have maturities ranging from immature to oil mature (Figures 4 and 5). However, in eleven of the Holywell Shale samples, low values for RockEval™ S₂ mean that kerogen type and maturity calculations are not accurate.

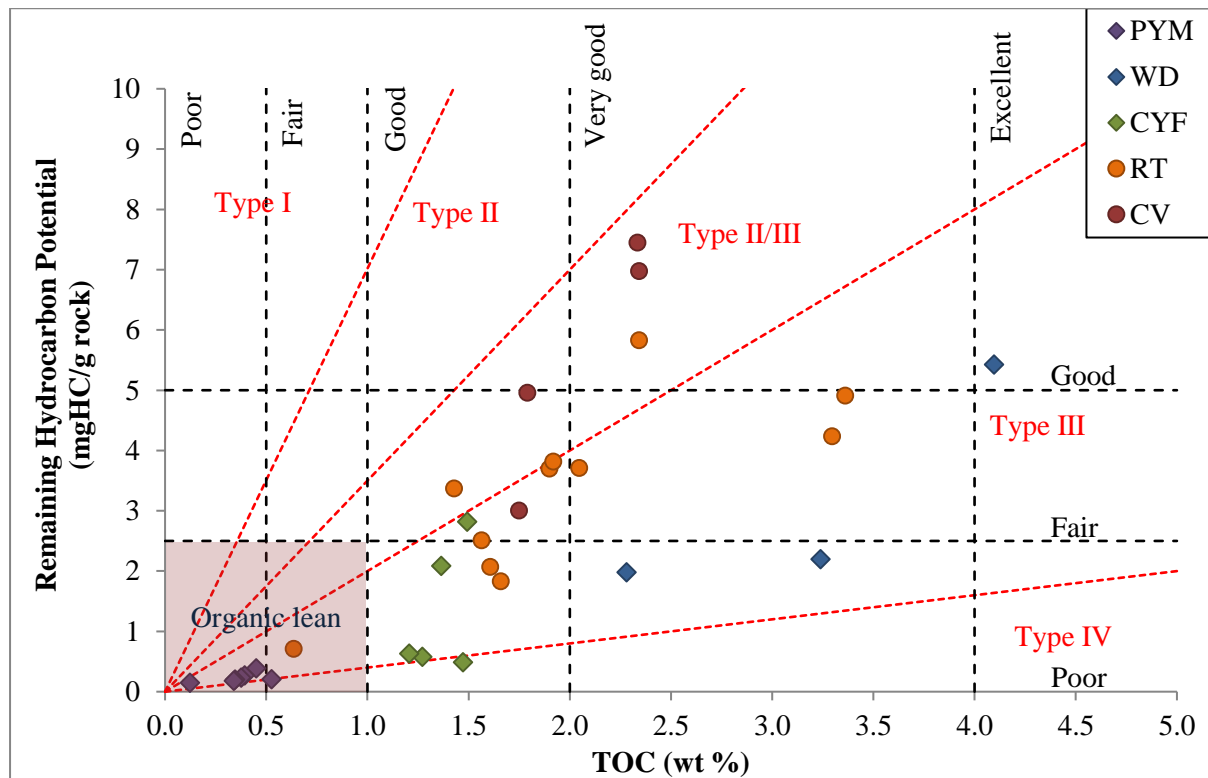


Figure 4: Kerogen quality plots indicating the kerogen type (in red) and generation ability of the remaining total organic matter (Y axis – which corresponds to S₂ from RockEval™). Warren Dingle (WD) sample WDS1H4 has been removed due to its high TOC value (10.31 wt %); it plots in the Type III kerogen region and is above good to excellent for TOC and remaining potential. The majority of samples are composed of type III kerogens; five samples (3 Cegidog Valley (CV) and 2 River Terrig (RT) samples) demonstrate a mixed type II/III kerogen, with 3 samples from Coed-y-Felin (CYF) exhibiting type IV kerogen (Table 1). PYM = Pen-Y-Maes. The shape of data points on the plot corresponds to Upper (diamond shape) and Lower (circle shape) Holywell Shale.

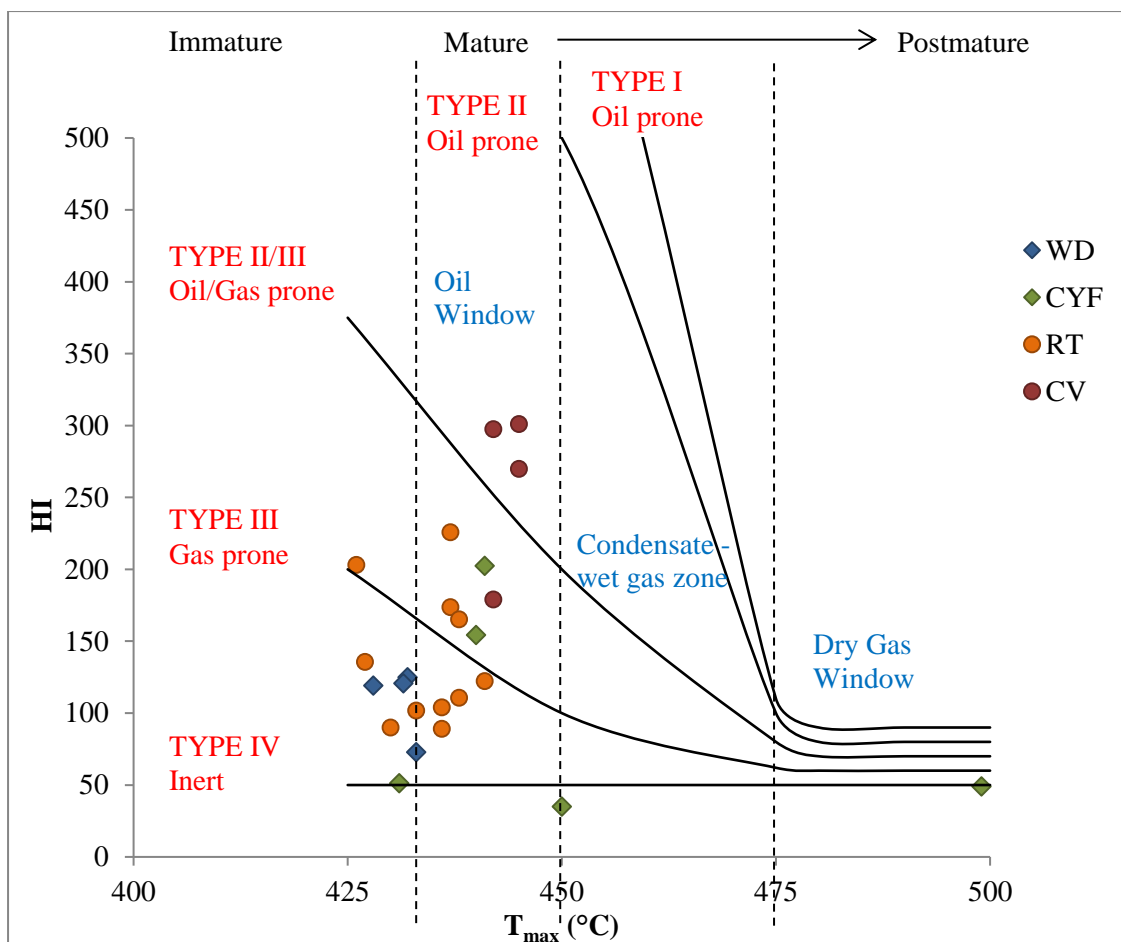


Figure 5: Plot of T_{max} and HI showing maturity and kerogen type. The T_{max} (x-axis) indicates the maturity the samples have reached and the black dotted lines indicate oil, condensate gas and dry gas windows. The majority of samples are immature to oil mature, with some Coed-Y-Felin (CYF) location samples showing anomalous HI and T_{max} values and Pen-Y-Maes (PYM) samples not included due to lack of organic matter present. RT = River Terrig; CV = Cegidog Valley. The shape of data points on the plot corresponds to Upper (diamond shape) and Lower (circle shape) Holywell Shale.

Carbon isotope signatures allow good insights to the provenance of the organic matter because terrestrially-derived kerogens in the Carboniferous have carbon isotopic values of -24 ‰ to -22 ‰ compared to -35 ‰ to -30 ‰ for marine organic matter (Lewan, 1986; Peters-Kottig et al., 2006; Stephenson et al., 2008). In this study, there is a clear difference in the range of carbon isotope values between the Lower and Upper Holywell Shale. $\delta^{13}C$ values in the Lower Holywell Shale range from -31.1 ‰ to -25.6 ‰ compared to -25.9 ‰ to -22.4 ‰ for the Upper

Holywell Shale. Based on the range of carbon isotope values in Table 1, we assume that terrestrial and marine organic matter have $\delta^{13}\text{C} = -22.5 \text{ ‰}$ and -31 ‰ respectively, so that organic matter in the Lower Holywell shale is 40-100 % marine and in the Upper Holywell is 0 – 40 % marine.

Using $\delta^{13}\text{C}$ as a proxy for the source of the organic matter, plots of $\delta^{13}\text{C}$ versus TOC and HI are shown in Figures 6 and 7 respectively. There is no relationship between the amount of organic matter and its source. And, whilst the end-member marine organic matter has higher HI values than the end-member terrestrial organic matter, the weak correlation between $\delta^{13}\text{C}$ and HI suggests variable degradation/preservation of both terrestrial and marine organic matter. Degradation of organic matter, either in the water column or at the seabed, is supported by the nitrogen contents of the sediments. A plot of total organic carbon versus total nitrogen shows a positive correlation and therefore implies that much of the sedimentary nitrogen is associated with organic matter (Figure 8). C/N ratios for marine organic matter typically range between 5 and 8 (Meyers et al., 2009). However, the C/N ratios for all samples (with the exception of Pen-Y-Maes) are in the range of 12.7 to 76.2 (Figure 9). Such high C/N ratios demonstrate the preservation of a carbon-rich, nitrogen-poor organic material which is most probably related, in these sediments, to the selective removal of nitrogen from organic matter during early diagenesis (Junium & Arthur, 2007; Meyers et al., 2009; Van Mooy et al., 2002; Verardo & MacIntyre, 1994; Meyers et al., 2009; Rivera & Quan, 2014). It is notable that organic matter at Pen-Y-Maes, which represents the terrestrial end-member, has the lowest C/N ratios, perhaps reflecting the initial ratio of the organic matter. Note also that the $\delta^{15}\text{N}$ data range from 1.2 to 3.2 ‰ but show no relationship to either the source or amount of organic matter (Calvert, 2004).

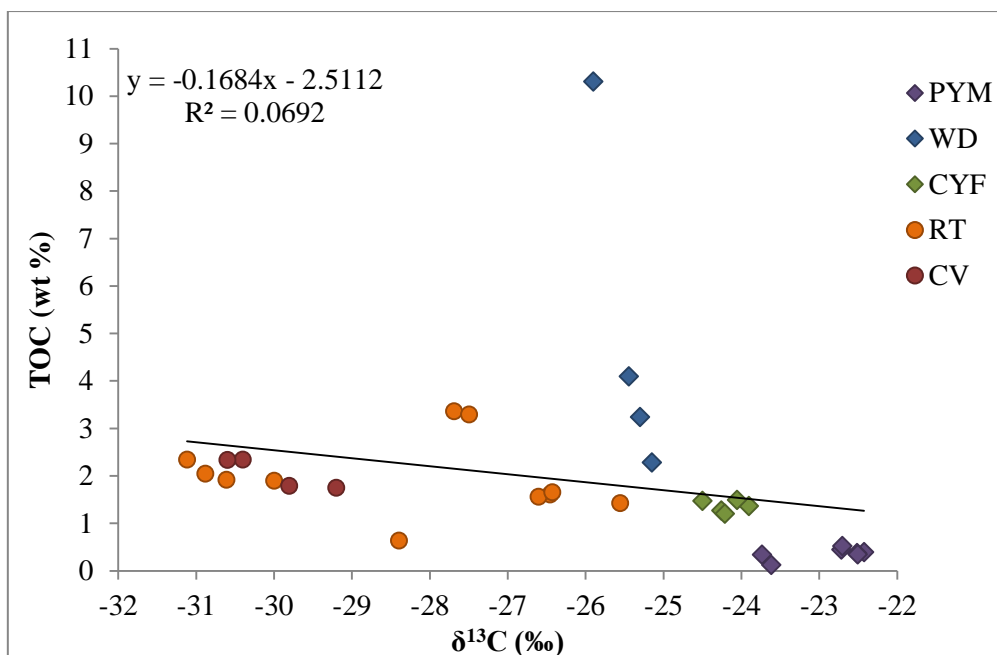


Figure 6: Total organic carbon versus carbon isotope composition of organic matter. Isotopically lighter results (-32 ‰) are indicative of a marine influence; isotopically heavier results (-22 ‰) indicate terrestrial organic matter. PYM = Pen-Y-Maes; WD = Warren Dingle; CYF = Coed-Y-Felin; RT = River Terrig; CV = Cegidog Valley. The shape of data points on the plot corresponds to Upper (diamond shape) and Lower (circle shape) Holywell Shale.

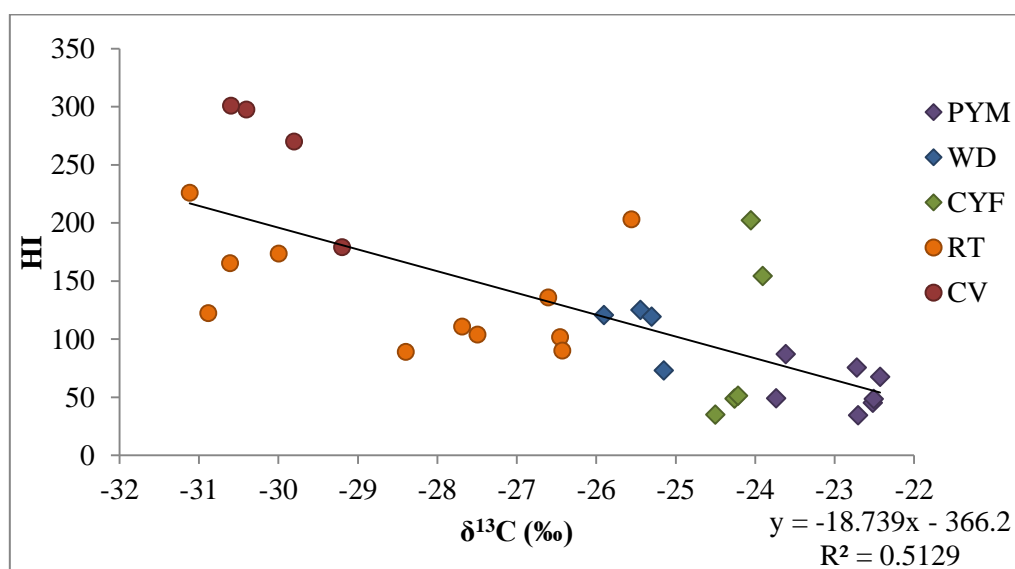


Figure 7: Hydrogen Index versus the carbon isotope composition of organic matter. PYM = Pen-Y-Maes; WD = Warren Dingle; CYF = Coed-Y-Felin; RT = River Terrig; CV = Cegidog Valley. The shape of data points on the plot corresponds to Upper (diamond shape) and Lower (circle shape) Holywell Shale.

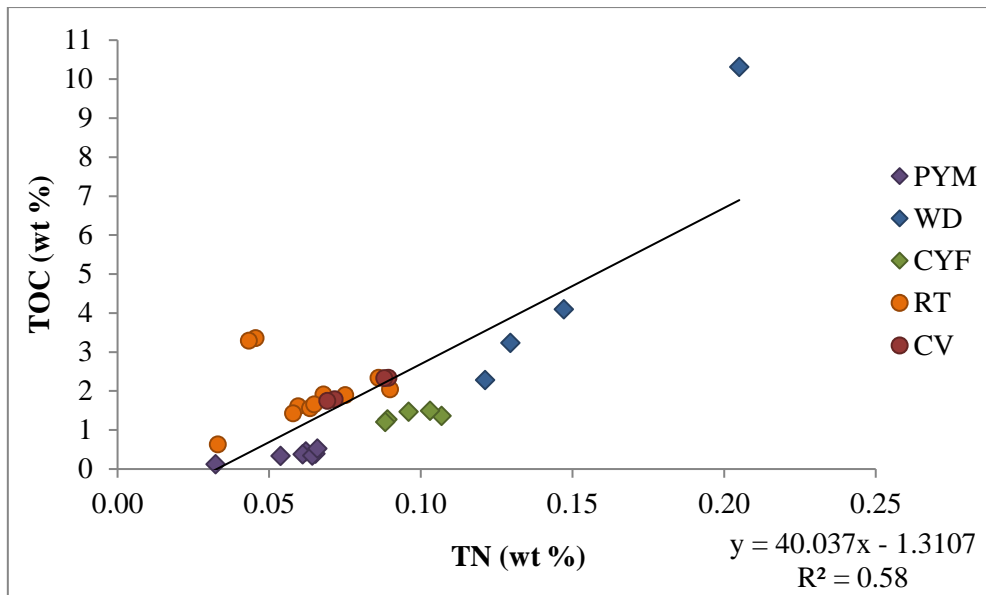


Figure 8: Total organic carbon versus total nitrogen. PYM = Pen-Y-Maes; WD = Warren Dingle; CYF = Coed-Y-Felin; RT = River Terrig; CV = Cegidog Valley. The shape of data points on the plot corresponds to Upper (diamond shape) and Lower (circle shape) Holywell Shale.

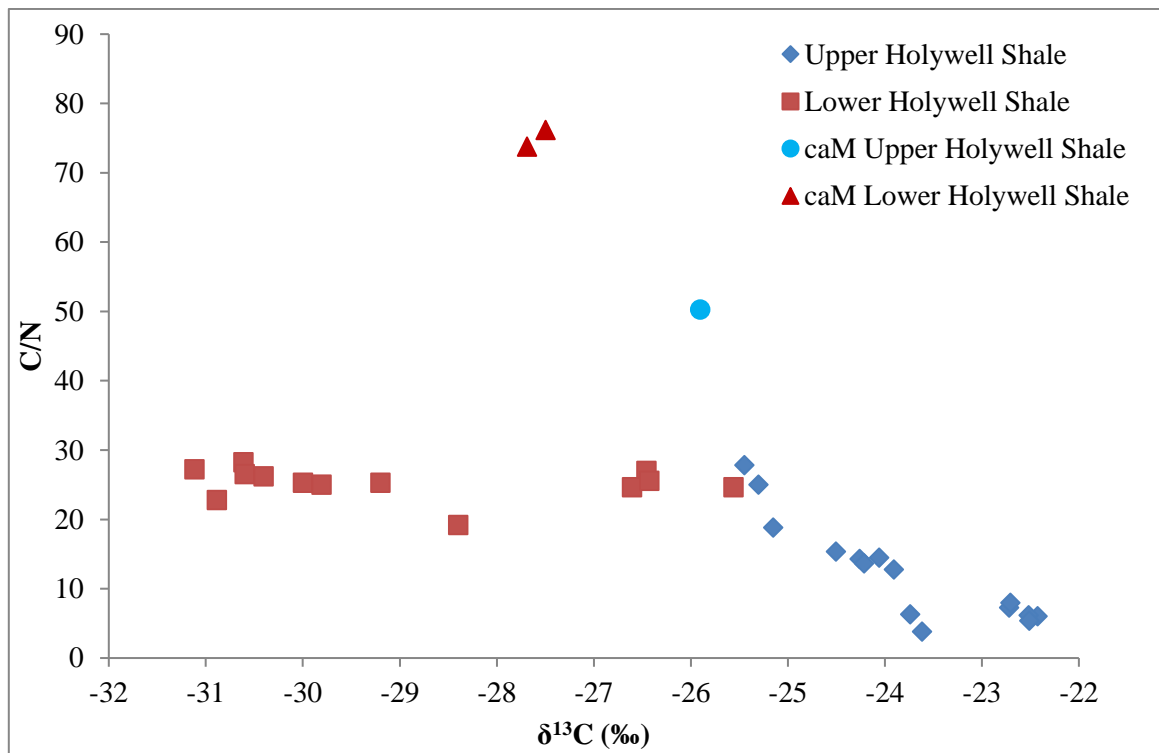


Figure 9: C/N ratio plotted with carbon isotope signature showing an increase in C/N with greater marine influence (more negative $\delta^{13}C$ ‰). The three outlying points with anomalously high C/N ratios have high CaO (from XRF) and are labelled caM = calcite rich mudstone.

3.2: Lithology, Mineralogy and Inorganic Geochemistry

Thin sections reveal a small number of centimetre-scale lithofacies including silt-rich and clay-rich mudstones; millimetre-scale, silt-clay bedding structures are common and are strong evidence of sediment transport (Figure 10). Around one third of the samples contain significant amounts of carbonate (Tables 2 and 3), some of which appears to be detrital (Figure 12A) and some of which is fossiliferous (Figure 10: facies 2). Carbonate, which is mainly calcite but includes some diagenetic dolomite and ferroan dolomite, occurs primarily in the Lower Holywell Shale, with detrital calcite most probably derived from erosion of pre-existing carbonate platforms (Arthurton et al., 1988; Gross et al., 2013; Johnson et al., 2001; Rose and Dunham, 1977; Waters et al., 2009).

There are no clearly-defined relationships between mineralogy, lithology and the nature and abundance of organic matter in this set of Holywell Shales. In the Upper Holywell Shale, samples from Pen-Y-Maes are silt-rich (Figure 10) and have low concentrations of terrestrial organic matter (Figure 7; Table 1). SEM studies show abundant, silt-grade detrital quartz and small amounts (less than 0.5 wt % TOC) of particulate organic matter, consistent with a terrestrial source (Figure 12B). Samples from Warren Dingle and Coed-Y-Felin have much lower Si/Al ratios and are thus more clay-rich. Compared to Pen-Y-Maes, they are substantially enriched in organic matter (1.2 wt % to 10.3 wt % TOC) and contain a mixture of terrestrial and marine organic matter, with up to 40 % marine organic matter (Figure 12C). The sample with 10.3 wt % TOC also contains almost 30 % calcite, including fossiliferous calcite.

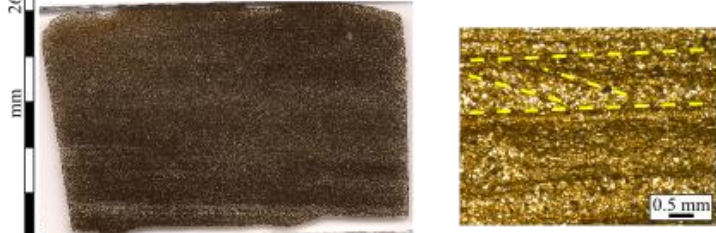
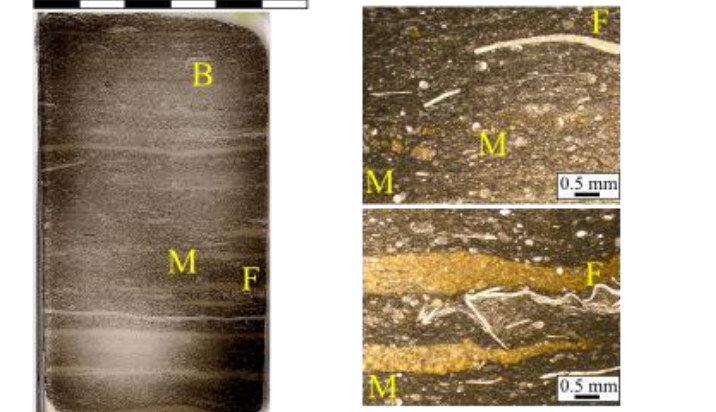
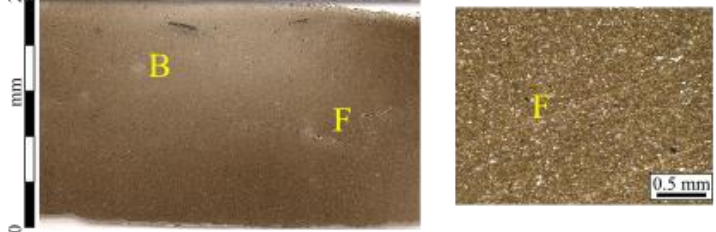
<p>Facies 1a: Silt-bearing mudstone - homogeneous</p> 	<p>n = 5 TOC: 0.1 wt % to 0.5 wt % $\delta^{13}\text{C}$: -23.6 ‰ to -22.4 ‰</p> <ul style="list-style-type: none"> • Silt sized (50 μm) sub-rounded detrital quartz grains. • Dark and light coloured clay and silt rich bands. • Fragmentary terrestrial organic matter. • Organic matter clustering in isolated lenses.
<p>Facies 1b: Silt-bearing- with graded bedding and sedimentary structures</p> 	<p>n = 2 TOC: 2.3 wt % to 0.3 wt % $\delta^{13}\text{C}$: -31.1 ‰ to -23.7 ‰</p> <ul style="list-style-type: none"> • Bedding grades from silt sized (50 μm) sub-rounded detrital calcite grains to clay sized (5 μm) calcite grains, occasional rounded quartz grain (<20 μm), and clusters of pyrite framboids. • Mixed, largely fragmentary organic matter (< 60 μm), with some amorphous organic matter aligning along bedding.
<p>Facies 2: Fossiliferous, calcareous, clay rich mudstone</p> 	<p>n = 4 TOC: 1.6 wt % to 10.3 wt % $\delta^{13}\text{C}$: -26.5 ‰ to -25.3 ‰</p> <ul style="list-style-type: none"> • Microfossils (micro-goniatites < μm) present. • Bone fragments present (μm). • Yellow stained bands under transmitted light. Composed of microfossil material. Yellow discolouration is possibly oil staining? • Amorphous organic matter aligns along bedding bending around larger grains along with clay minerals. • Discrete lenses and subtle continuous wavy lamination. Often lenticular fabric and beds distorting around fossils and large detrital grains. • Burrows present, often calcite filled.
<p>Facies 3a: Clay rich mudstone – homogeneous</p> 	<p>n = 2 TOC: 3.4 wt % to 3.3 wt % $\delta^{13}\text{C}$: -27.7 ‰ to -27.5 ‰</p> <ul style="list-style-type: none"> • Massive/homogenous texture with no signs of bedding. • Often bioturbated with burrows present. • Mixed fragmentary and amorphous organic matter (< 20 μm).
<p>Facies 3b: Clay rich mudstone – with discrete graded bedding and wavy lamination</p> 	<p>n = 9 TOC: 1.2 wt % to 2.3 wt % $\delta^{13}\text{C}$: -30.6 ‰ to -23.9 ‰</p> <ul style="list-style-type: none"> • Graded bedding with continuous parallel beds and continuous non-parallel wavy beds. • Small grain size and thinner beds compared with facies 1b

Figure 10: Lithofacies within the Holywell Shale, thin section image and transmitted light image showing example of each individual facies. Example lithofacies are from both Upper and Lower Holywell Shale samples (facies 1a: PYMS2H3; facies 1b: RTS5H1 & PYMS1H5; facies 2: WDS1H4; facies 3a: RTS6H1; facies 3b: CVS3H2). Each lithofacies description includes the number of samples which have that lithofacies description (n), a range of TOC and $\delta^{13}\text{C}$ values identified within the Holywell Shale. Vertical arrow = fining upward sequence with increase in clay toward the top, inclined arrow = example of bedding feature such as lens, wavy lamination, small scale cross-bedding, M = microfossil, F = bone or shell fragment, B = burrow.

It is possible to estimate clay mineral content for the Holywell Shale samples using Si/Al. A value for Si/Al from average shale based on 277 samples is 3.1, with clay mineral content around 60% (Ross & Bustin, 2009; Wedepohl, 1971). The Si/Al ratios for the Upper Holywell Shale are between 2.5 and 5 whereas the Lower Holywell Shale samples have Si/Al ratios from 5 to 15. This would suggest that the Lower Holywell Shale has clay mineral contents considerably lower than 60%, whereas the Upper Holywell Shale samples from Warren Dingle and Coed-Y-Felin locations have clay mineral contents higher than 60%.

In the Lower Holywell Shale, samples from Cegidog Valley contain primarily marine organic matter, with TOC contents between 1.8 and 2.4 wt % (Table 1). Scanning electron micrographs indicate the presence of laminar organic matter and also abundant silt-grade detrital quartz (Figure 12D). Whilst it is difficult to differentiate detrital and diagenetic quartz without cathodoluminescence data (Milliken et al., 2012; Schieber, 2000), textural evidence suggests that some quartz grains may be recrystallized biogenic silica (Figure 12E).

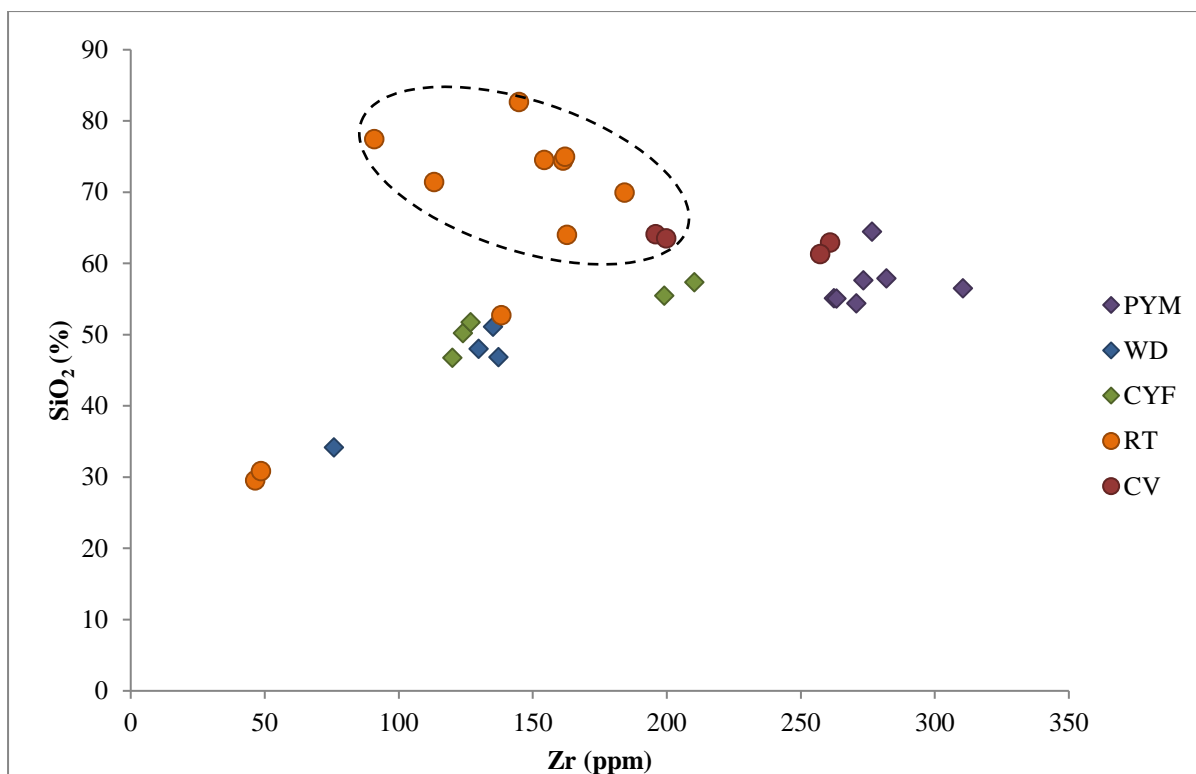


Figure 11: SiO₂ versus Zr. The strong correlation in most of the sample set is taken to indicate that the quartz is mainly or entirely detrital. Samples from River Terrig and Cegidog Valley are highlighted by the dashed oval line and are relatively enriched in silica, suggesting an input of biogenic silica in addition to detrital quartz. The shape of data points on the plot corresponds to Upper (diamond shape) and Lower (circle shape) Holywell Shale.

Lower Holywell Shale samples from River Terrig contain 0.6 - 3.4 wt % TOC (Table 1). The organic matter is 40-100 % marine and there is no relationship between the source and amount of organic matter. Samples from River Terrig have the highest Si/Al ratios of the whole sample set, with SiO₂ contents up to 83 % (Table 3). From a geomechanical and petrophysical perspective, it is important to understand whether the quartz is detrital or diagenetic, since the recrystallization of biogenic silica to quartz can lithify and strengthen the mudstone, with important consequences from the formation of hydraulic fractures (Jarvie et al., 2007). SEM evidence suggests that much of the quartz is detrital rather than diagenetic, with silt-grade and sometimes sand-grade quartz grains associated with a clay matrix (Figure 12F). Figure 11

shows that eight samples from River Terrig are enriched in SiO₂ relative to Zr and are likely to contain some biogenically sourced quartz, samples from other areas only have quartz from detrital sources. The poor sorting of some samples from River Terrig suggests that they may have been deposited from mass wasting processes; in addition, some samples contain substantial carbonate which, based on its similar grain size to quartz, may have a detrital origin supplied from erosion of the underlying Clwyd Limestone.

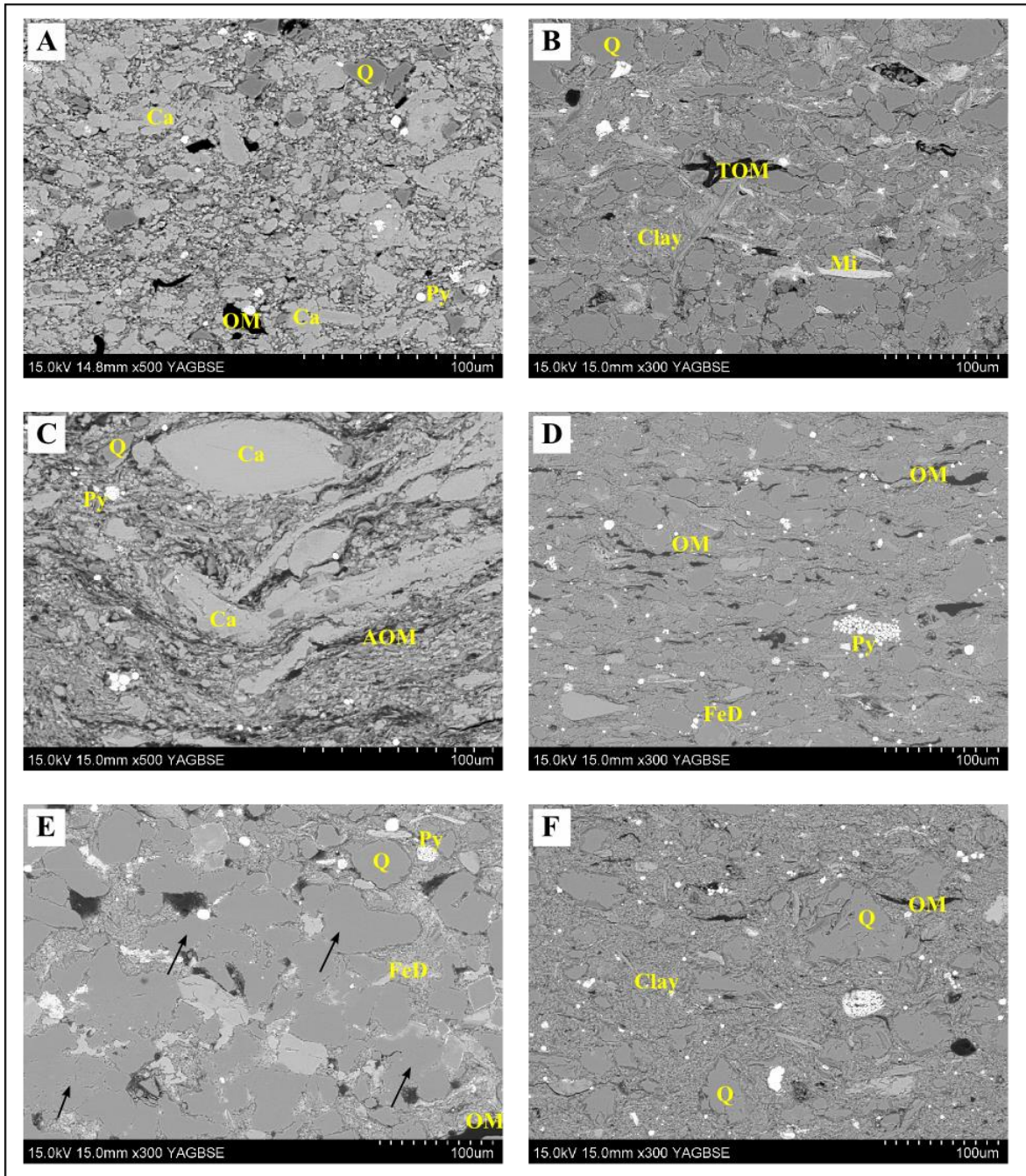


Figure 12: Backscatter electron microscope images of the Holywell Shale. Q = quartz, Ca = carbonate, Py = pyrite, OM = organic matter, AOM = amorphous, TOM = terrestrial, Mi = mica, FeD = ferroan dolomite. A (sample RTS6H1): sample rich in detrital carbonate grains; B (sample PYMS1H5): sample with large detrital quartz grains; C (sample WDS1H4): carbonate grains occurring with large amounts of AOM; D (sample CVS2H1): laminar organic matter with abundant silt sized quartz; E (sample CVS3H2): black arrows denote possible diagenetic quartz (possibly from remineralisation of biogenic silica), with some other diagenetic minerals such as

ferroan dolomite; F (sample RTS5H1): large (sand/silt sized) detrital grains of quartz within a fine clay matrix.

Trace element data are shown in Table 4. Here, we are particularly interested in trace elements which give insights to redox conditions at the sediment-water interface or the occurrence of sulphidic bottom- or pore-waters. In general, abundances of elements such as uranium, vanadium and zinc, are similar to those seen in average shale and generate no support for oxygen-depleted bottom waters (e.g. Jones and Manning, 1994). In detail, higher uranium concentrations and U/Th ratios in samples from Warren Dingle and some from River Terrig occur are typically higher in TOC and CaCO₃ than other samples, implying that these may be periods or areas where primary productivity was higher and/or where bottom water oxygen concentrations may have been reduced from fully saturated conditions.

4. Discussion:

4.1 Depositional System

The combination of organic geochemical, inorganic geochemical and petrographic data indicate that controls on (a) organic matter quantity and quality and (b) lithology in the Holywell are complex and vary substantially on a wide range of spatial and temporal scales. Shale reservoir quality, which is largely controlled by these parameters, is thus highly variable and inherently difficult to predict.

Generally, and throughout the whole period of Holywell Shale deposition, a mixture of terrestrial and marine organic matter was supplied to a range of marine depositional environments in which there was sufficient hydrodynamic energy to transport fine-grained sediment as bed load. The resulting mudstones exhibit a range of sedimentary textures with millimetre- to centimetre-scale silt-clay bed forms but which show almost no relationship

between texture and organic matter type or amount. Trace element data, high C/N ratios and low HI values all indicate oxygenated bottom waters which allowed substantial degradation of organic matter at or close to the seabed, resulting in the poor preservation of organic matter and relatively low petroleum potentials. The combination of the early diagenetic destruction of organic matter plus its dual supply from both terrestrial and marine sources has resulted in weak relationships between the quantity and quality of preserved organic matter, and also between lithology and the organic matter amount and type. Similar observations were made by Davies et al. (2012) in a Marsdenian mud-rich sequence approximately 150 kilometres further north, albeit in an area more dominated by a terrestrial organic matter source.

Within this general framework, there are important details in the data. Organic matter in the lowermost (E2a age; *E. bisulcatum*) Holywell Shale, at Cegidog Valley, is dominantly marine. Based on its relatively low C/N ratio and relatively high HI, the organic matter is moderately well preserved. Abundances of silica and phosphate are higher than those in samples from other localities, there is petrographic evidence for recrystallized biogenic silica (Figure 12E) and SiO₂/Zr ratios are slightly elevated compared to samples with purely detrital quartz. These characteristics suggest that primary productivity may have been elevated in this area at this time, but that relatively little organic matter (average 2.2 wt %) was preserved due to the oxygenated bottom waters indicated by, for example, low sedimentary uranium contents, low U/Th, V/Cr, and Ni/Co ratios (averages 0.25, 0.67, 0.37 respectively; Table 4). In contrast, organic matter in Armstrong et al.'s (1997) study of E2a age samples from the Hope Mountain area 3 km east of Cegidog Valley has $\delta^{13}\text{C}$ values of -25.5 ‰, indicating a predominantly terrestrial source. Such a large isotopic difference over such a small distance suggests that supplies of organic matter were highly variable and resulted in quite different organofacies.

There is similar evidence (fossiliferous calcite; phosphate) for elevated primary productivity from the lower part of the sample set from River Terrig. Nevertheless, organic matter in the two most calcite-rich samples is only 40 % marine, implying a significant supply of terrestrial organic matter. Preservation of organic matter, based on very high C/N ratios and HI values of around 100-150, is poor, indicating substantial destruction close to the sediment-water interface.

Elevated values of primary productivity are common where upwelling occurs on continental margins. Whilst we cannot prove this with our data, we do note that the study area was situated at the southwest edge of the Pennine Basin. Furthermore, it is notable that some of the quartz in River Terrig samples comprises sand-size grains which float in a clay matrix (Figure 12F) which could be interpreted as deposition from downslope depositional processes such as mass wasting. We also recognise that these observations are consistent with other interpretations, including the lateral transport of clay-sand floes as bedload on continental shelves (Schieber et al., 2007; 2010; Davies et al., 2012).

Organic matter in the Upper Holywell shale is predominantly terrestrial but with a marine contribution up to 40 % (assuming that terrestrial and marine organic matter have $\delta^{13}\text{C} = -22.5$ ‰ and -31 ‰ respectively, 40% is the greatest potential marine contribution from carbon isotope values of -25.9 ‰). The more clay-rich samples, for example at Warren Dingle, are enriched in organic matter (2.2 – 10.8 wt %) and also have the greatest contribution of marine organic matter. The most organic-rich sample also contains fossiliferous carbonate and phosphate, suggesting a period of higher biological productivity; nevertheless, the high C/N ratio and low HI indicates an oxygenated depositional environment which was not conducive to the preservation of hydrogen-rich organic matter. Given their similar hydrodynamic properties, we infer that the coincidence of relatively elevated clay mineral and organic matter

contents relate to hydrodynamic sorting, perhaps related to bedload transport across continental shelves (e.g. Tyson & Follows, 2000).

The silt-rich samples from Pen-y-Maes have less than 0.5 wt % TOC which is isotopically heavy and comprises angular, terrestrially sourced organic matter fragments. This facies is very similar to the Marsdenian silt-bearing, clay-rich mudstones with graded beds described by Davies et al. (2012). This litho/organofacies, deposited at the very end of the Namurian, represents a more proximal facies deposited at a time when major deltas were prograding from the north, ultimately depositing the Gwespys sandstones in the Yeadonian and early Westphalian.

4.2 Reservoir Quality

The Holywell Shale was deposited in a relatively shallow water environment into which organic matter was supplied from both terrestrial and marine sources and in which the transport of fine-grained sediment was a dominant process. These complex, coupled processes resulted in a sediment system which is heterogeneous, in terms of both lithofacies and organofacies, on many spatial scales. There are no simple rules to describe relationships between lithofacies, mineralogy and organic matter amount and type. Equally, since shale reservoir quality relates to both gas storage (TOC, porosity) and gas delivery (mineralogy and induced fracture characteristics, permeability), there are no simple rules with which to predict reservoir quality in space and time. These rocks are dominantly clastic and are mixtures of silt-grade and clay-grade particles. Silt-rich units have high matrix permeabilities and will contribute to gas delivery, whereas clay-rich units have much lower permeabilities (Dewhurst et al., 1998; Yang and Aplin, 2007; 2010); silt-clay interbeds are highly anisotropic with respect to permeability (Armitage et al., 2011). Units of all these types occur in each part of the Holywell Shale, on

many spatial scales. Connecting the silt-rich parts of the system should enhance the large-scale permeability of the reservoir.

In terms of mineralogy and the way in which mudstones respond to hydraulic fracturing practices, recrystallized biogenic calcite and silica are often considered to embrittle fine-grained sediments and thus to enhance reservoir quality. Whilst calcite occurs in some of the Holywell Shale, abundances are typically less than 10%. Silica concentrations are very variable but reach up to 82% in some samples from the Lower Holywell Shale. However, it is unclear how much of the silica has a biogenic source. Our petrographic observations suggest that most silica is macroscopic and detrital, although a contribution from biogenic silica is certainly possible.

Hydrocarbons in shales are generally considered to be stored both as free oil/gas within the pore system and as adsorbed oil/gas associated with organic matter (e.g. Montgomery et al., 2005; Gasparik et al., 2012; Rexer et al., 2013). Organic matter contents in the Holywell Shale only average 1.9 wt % and only a small portion of the Formation has TOC contents above 3 wt %. Silt-rich units represent the best reservoir quality in terms of permeability but are often depleted in organic matter. The prospectivity of silt-rich units is thus dependent on migration, trapping and sealing, as for a conventional play. In this context the Holywell Shale might be considered as a hybrid play (Jarvie, 2011). Whilst the Holywell Shale is immature to early oil mature, age equivalent units within the UK range from immature to mature for gas generation due to the complex tectonic, depositional and burial history of the Carboniferous Pennine Basin (Andrews, 2013; Gross et al., 2015; Słowakiewicz et al., 2015).

Conclusions:

The Holywell Shale represents a mudstone sequence with highly variable organofacies and lithofacies which was deposited along the south western edge of the Pennine Basin during the Namurian (Carboniferous). The continued progradation of the Namurian delta systems, combined with a reduced thermal subsidence rate, led to a reduction in accommodation space and an increase in the importance of terrestrially derived minerals and organic matter.

Organic and inorganic geochemical data, along with petrographic observations, demonstrate the highly variable supply and preservation of organic matter and lithology in the Holywell Shale. The general trend is a reduction in the amount of marine sourced organic matter from the Lower to Upper Holywell Shale, but with large spatial variations in organic matter supply at a given time. There is no relationship between amount of organic matter and its source.

The combination of mixed organic matter sources, poor preservation conditions along with early diagenetic destruction of organic matter mean that there are only weak relationships between organic matter quality and quantity. There are also only weak links between organic matter quantity, type and lithology. Trace element data, combined with low HI and high C/N ratios indicate oxygenated bottom waters which resulted in poorly preserved organic matter, despite an average TOC content of 1.9 wt %. Type II/III kerogens dominate the Lower Holywell Shale with Type III/IV in the Upper Holywell Shale. The greatest petroleum potential is found within the Lower Holywell Shale samples during periods or areas of higher primary productivity and reduced bottom water oxygen levels. The complexity of the sedimentary system in both space and time means that shale reservoir quality is inherently difficult to predict.

Acknowledgments:

The authors would like to acknowledge: IGas Energy Plc for providing the funding for this research. Martin Jones at Newcastle University for providing RockEval™ analysis; John

Martin and Alex Finlay at Chemostrat Ltd for the XRF analysis; three anonymous reviewers whose comments improved the manuscript.

Appendix:

Table 1: Geochemical data from all locations: TOC, Carbon isotopes ($\delta^{13}\text{C}$), RockEval™ primary and secondary parameters (S_1 , S_2 , T_{max} , HI, PI, TI, PY), Calc %Ro (Calculated vitrinite reflectance equivalent, $\text{VRO}\% = 0.018 \times T_{\text{max}} - 7.16$ from Jarvie et al., 2001), Kerogen Type (from RockEval™), TN, C/N, $\delta^{15}\text{N}$; BET surface area data is also included in the chart.

	Sample	TOC (wt %)	$\delta^{13}\text{C}$ (‰)	S_1 (mg/g)	S_2 (mg/g)	T_{max} (°C)	HI	PI	TI	PY	Calc %Ro	Kerogen Type	BET Surface Area (m ² /g)	TN (wt %)	C/N	$\delta^{15}\text{N}$ (‰)	S (%)
Upper Holywell Shale	PYMS1H1	0.45	-22.7	0.10	0.39	386	75	0.20	0.21	0.49	**	N/A	5.86	0.06	8.33	2.5	0.01
	PYMS1H2	0.39	-22.4	0.10	0.27	**	68	0.27	0.25	0.37	**	N/A	0.40	0.07	6.12	1.6	0.00
	PYMS1H3	0.38	-22.5	0.08	0.24	**	45	0.25	0.21	0.32	**	N/A	0.73	0.06	8.53	3.1	0.00
	PYMS1H4	0.35	-22.5	0.08	0.20	**	49	0.29	0.23	0.28	**	N/A	0.68	0.06	6.41	2.2	0.01
	PYMS1H5	0.34	-23.7	0.06	0.18	312	49	0.25	0.18	0.24	**	N/A	0.60	0.05	6.84	3.0	0.00
	PYMS2H1	0.53	-22.7	0.07	0.21	529	35	0.25	0.13	0.28	**	N/A	0.64	0.07	9.21	3.1	0.01
	PYMS2H2	0.12	-23.6	0.06	0.15	**	87	0.29	0.49	0.21	**	N/A	0.36	0.03	5.33	2.9	0.01
	WDS1H1	4.10	-25.5	0.40	5.43	432	125	0.07	0.10	5.83	0.62	III	16.87	0.15	29.51	2.2	0.37
	WDS1H2	3.24	-25.3	0.30	2.20	428	119	0.12	0.09	2.50	0.54	III	2.98	0.13	14.25	2.6	1.03
	WDS1H3	2.28	-25.2	0.29	1.98	433	73	0.13	0.13	2.27	0.63	III	18.89	0.12	22.41	2.6	0.08
	WDS1H4	10.31	-25.9	0.94	16.09	432	121	0.06	0.09	17.03	0.61	III	2.80	0.21	65.10	1.2	0.78
	CYFS1H1	1.27	-24.3	0.13	0.58	499	49	0.18	0.10	0.71	1.82	N/A	1.56	0.09	13.32	3.0	2.92
	CYFS1H2	1.37	-23.9	0.17	2.09	440	154	0.08	0.12	2.26	0.76	III	6.54	0.11	12.67	2.8	0.03
	CYFS1H2i	1.49	-24.1	0.20	2.82	441	202	0.07	0.13	3.02	0.78	III	6.33	0.10	13.52	2.6	0.02
	CYFS1H3	1.21	-24.2	0.17	0.63	431	51	0.21	0.14	0.80	0.60	N/A	1.57	0.09	13.94	3.2	2.84
	CYFS1H4	1.47	-24.5	0.17	0.49	450	35	0.25	0.11	0.66	0.94	N/A	17.00	0.10	14.63	2.9	0.71
Lower Holywell Shale	RTS1H2	2.05	-30.9	0.19	3.71	441	122	0.05	0.09	3.90	0.78	III	11.81	0.09	33.80	2.4	0.05
	RTS1H3	1.90	-30.0	0.14	3.70	437	174	0.04	0.07	3.84	0.71	III	10.94	0.08	28.40	2.9	0.04
	RTS1H4	1.92	-30.6	0.18	3.82	438	165	0.05	0.09	4.00	0.72	III	8.79	0.07	34.04	2.8	0.04
	RTS1H5	0.63	-28.4	0.09	0.71	436	89	0.11	0.14	0.80	0.69	N/A	4.68	0.03	23.99	2.6	0.02
	RTS2H1	1.61	-26.5	0.21	2.07	433	102	0.09	0.13	2.28	0.63	III	7.39	0.06	34.19	3.0	0.43
	RTS2H2	1.56	-26.6	0.26	2.51	427	136	0.09	0.17	2.77	0.53	III	13.34	0.06	29.15	3.2	0.03
	RTS2H3	1.43	-25.6	0.46	3.37	426	203	0.12	0.32	3.83	0.51	II/III	8.40	0.06	28.68	2.9	0.03
	RTS2H4	1.66	-26.4	0.22	1.83	430	90	0.11	0.13	2.05	0.58	III	10.46	0.06	31.12	2.6	0.27
	RTS3H1	3.36	-27.7	0.23	4.91	438	111	0.04	0.07	5.14	0.72	III	5.20	0.05	97.25	2.3	0.37
	RTS5H1	2.34	-31.1	0.11	5.83	437	226	0.02	0.05	5.94	0.71	II/III	3.37	0.09	29.99	2.0	0.11
	RTS6H1	3.30	-27.5	0.26	4.24	436	104	0.06	0.08	4.50	0.69	III	2.82	0.04	94.16	2.3	0.30
	CVS1H1	2.34	-30.4	0.23	6.98	442	298	0.03	0.10	7.21	0.80	II/III	8.57	0.09	26.26	2.9	0.94
	CVS2H1	2.33	-30.6	0.25	7.45	445	301	0.03	0.11	7.70	0.85	II/III	11.91	0.09	28.13	2.9	0.72
	CVS3H1	1.79	-29.8	0.21	4.96	445	270	0.04	0.12	5.17	0.85	II/III	7.57	0.07	25.66	3.2	0.35
CVS3H2	1.75	-29.2	0.15	3.01	442	179	0.05	0.09	3.16	0.80	III	7.04	0.07	24.29	3.0	0.38	

Table 2: Qualitative XRD results minerals identified in each sample (x represents mineral is present, - represents mineral absent from sample).

	Sample	Quartz	Illite	Kaolinite	Chlorite	Calcite	Pyrite	Albite
Upper Holywell Shale	PYMS1H1	x	x	x	x	-	-	x
	PYMS1H2	x	x	x	x	-	-	x
	PYMS1H3	x	x	x	x	-	-	x
	PYMS1H4	x	x	x	x	-	-	x
	PYMS1H5	x	x	x	x	-	-	x
	PYMS2H1	x	x	x	x	-	-	x
	WDS1H1	x	x	x	-	-	x	-
	WDS1H2	x	x	x	-	-	x	-
	WDS1H3	x	x	x	-	-	-	-
	WDS1H4	x	x	x	x	x	x	-
	CYFS1H1	x	x	x	x	-	x	-
	CYFS1H2	x	x	x	x	-	-	-
	CYFS1H2i	x	x	x	x	-	-	-
	CYFS1H3	x	x	x	x	-	x	-
	CYFS1H4	x	x	x	x	-	-	-
	Lower Holywell Shale	RTS1H2	x	x	-	-	-	-
RTS1H3		x	x	-	-	-	-	-
RTS1H4		x	x	-	-	-	-	-
RTS1H5		x	x	x	-	-	-	-
RTS2H1		x	x	x	x	x	-	-
RTS2H2		x	x	-	-	-	-	-
RTS2H3		x	x	-	-	-	-	-
RTS2H4		x	x	x	x	x	x	-
RTS3H1		x	x	x	x	x	x	-
RTS5H1		x	x	-	-	-	-	-
RTS6H1		x	x	-	-	x	-	-
CVS1H1		x	x	x	-	-	x	-
CVS2H1		x	x	x	-	-	x	-
CVS3H1		x	x	x	-	-	x	-
CVS3H2	x	x	x	x	-	x	-	

Table 3: Quantitative XRF results with major geological elements and their oxides identified.

		Al ₂ O ₃ (%)	SiO ₂ (%)	TiO ₂ (%)	Fe ₂ O ₃ (%)	MnO (%)	MgO (%)	CaO (%)	Na ₂ O (%)	K ₂ O (%)	P ₂ O ₅ (%)	Si/Al	Zr/Al
Upper Holywell Shale	PYMS1H1	16.03	57.90	1.01	5.61	0.06	1.78	0.11	0.57	2.58	0.12	3.61	17.59
	PYMS1H2	16.01	57.64	1.01	5.34	0.05	1.75	0.17	1.04	2.54	0.11	3.60	17.07
	PYMS1H3	16.84	55.10	1.02	5.78	0.04	1.88	0.40	0.86	2.57	0.13	3.27	15.58
	PYMS1H4	16.69	54.41	1.04	5.82	0.06	1.94	0.33	0.57	2.68	0.16	3.26	16.22
	PYMS1H5	16.29	56.53	1.00	5.48	0.09	1.77	0.41	0.84	2.31	0.13	3.47	19.06
	PYMS2H1	16.43	55.09	1.01	6.03	0.15	1.87	0.39	0.73	2.56	0.14	3.35	16.02
	PYMS2H2	12.99	64.47	0.79	4.04	0.04	1.46	0.21	1.27	1.66	0.07	4.96	21.30
	WDS1H1	18.66	48.02	0.82	6.61	0.06	1.44	0.46	0.00	3.12	0.14	2.57	6.95
	WDS1H2	18.22	46.83	0.83	5.90	0.02	1.48	0.26	0.00	3.57	0.10	2.57	7.53
	WDS1H3	19.25	51.13	0.86	7.19	0.01	1.61	0.24	0.00	3.63	0.15	2.66	7.02
	WDS1H4	12.32	34.17	0.51	3.95	0.15	1.40	15.58	0.00	2.11	1.69	2.77	6.15
	CYFS1H1	18.48	46.75	0.80	7.02	0.10	1.74	0.31	0.00	2.77	0.04	2.53	6.49
	CYFS1H2	19.48	55.46	1.07	3.67	0.02	2.03	0.26	0.00	3.46	0.02	2.85	10.22
	CYFS1H2i	18.96	57.37	1.02	3.44	0.02	2.02	0.27	0.00	3.26	0.02	3.03	11.09
	CYFS1H3	19.50	50.23	0.82	6.96	0.11	1.98	0.33	0.00	2.78	0.06	2.58	6.35
	CYFS1H4	19.60	51.75	0.88	3.81	0.01	1.43	0.12	0.00	3.07	0.01	2.64	6.47
Lower Holywell Shale	RTS1H2	7.84	74.43	0.49	2.42	0.00	0.99	0.06	0.00	2.11	0.32	9.49	20.57
	RTS1H3	10.24	69.93	0.60	1.95	0.00	1.32	0.06	0.00	2.72	0.32	6.83	17.99
	RTS1H4	8.46	74.53	0.51	1.92	0.00	1.04	0.09	0.00	2.26	0.33	8.81	18.22
	RTS1H5	5.54	82.68	0.35	1.57	0.00	0.54	0.13	0.00	1.33	0.35	14.91	26.12
	RTS2H1	11.40	52.74	0.72	3.01	0.04	1.92	9.83	0.00	3.01	0.20	4.62	12.12
	RTS2H2	9.05	71.45	0.54	2.80	0.02	1.23	0.32	0.00	2.21	0.10	7.89	12.50
	RTS2H3	8.81	77.45	0.50	1.10	0.00	1.02	0.07	0.00	2.21	0.00	8.79	10.31
	RTS2H4	12.90	64.03	0.83	3.68	0.02	1.94	2.60	0.00	3.39	0.06	4.96	12.61
	RTS3H1	6.04	29.56	0.32	2.04	0.12	1.39	29.03	0.00	1.51	0.46	4.89	7.69
	RTS5H1	8.58	74.96	0.52	2.01	0.00	1.09	0.06	0.00	2.35	0.29	8.73	18.88
	RTS6H1	6.07	30.84	0.29	2.16	0.13	1.33	27.69	0.00	1.53	0.32	5.08	8.01
	CVS1H1	9.86	64.12	0.61	3.52	0.03	2.22	1.93	0.00	2.66	0.23	6.50	19.86
	CVS2H1	9.55	63.51	0.60	3.28	0.03	2.52	2.69	0.00	2.63	0.28	6.65	20.91
	CVS3H1	10.22	62.92	0.66	3.82	0.06	2.48	2.35	0.00	2.65	0.29	6.16	25.52
CVS3H2	10.34	61.32	0.67	3.89	0.06	2.59	3.41	0.00	2.68	0.29	5.93	24.86	

Table 4: Trace element results from XRF all results are reported as ppm (parts per million).

	As	Ba	Ce	Co	Cr	Cu	Ga	La	Nb	Ni	Pb	Rb	Sr	Th	U	V	Y	Zn	Zr
PYMS1H1	10.0	407.2	105.3	12.3	90.3	39.0	14.8	44.7	14.7	36.1	15.8	108.5	98.3	11.0	1.6	100.2	36.1	86.1	282.0
PYMS1H2	11.0	371.3	94.9	10.8	82.5	32.3	15.5	52.0	15.4	36.0	7.4	106.4	103.8	10.6	1.2	102.1	37.7	71.1	273.3
PYMS1H3	10.2	385.9	114.5	17.2	95.6	33.2	16.0	58.2	15.2	43.9	8.1	106.3	111.4	11.9	1.1	94.0	36.3	71.9	262.4
PYMS1H4	10.5	388.4	78.6	20.4	85.0	33.4	15.8	52.7	15.4	42.8	8.8	106.2	108.7	11.6	2.4	102.0	39.0	86.2	270.7
PYMS1H5	11.2	399.1	82.2	14.1	81.2	26.2	16.1	42.8	14.8	39.0	6.5	97.0	106.7	12.1	1.8	102.7	35.7	69.5	310.5
PYMS2H1	17.3	487.4	100.4	17.5	88.8	35.1	17.4	38.7	15.1	47.5	12.3	109.1	107.0	11.9	2.0	77.5	36.9	91.7	263.3
PYMS2H2	6.0	275.8	66.2	9.0	63.5	25.2	9.5	33.9	11.0	27.1	27.4	60.7	74.0	5.9	LOD	54.3	27.6	63.7	276.6
WDS1H1	61.1	514.7	122.5	25.6	168.6	114.5	24.1	57.4	11.3	108.3	102.0	163.1	68.1	13.5	10.8	290.0	62.8	57.5	129.7
WDS1H2	42.2	487.7	91.6	14.3	139.2	176.2	22.4	43.8	12.7	63.5	63.5	182.0	70.0	14.6	8.7	234.7	33.7	49.5	137.2
WDS1H3	39.5	549.8	93.0	24.6	147.3	81.6	24.3	42.2	12.5	46.2	52.4	183.1	71.2	15.1	6.9	228.3	33.0	55.3	135.1
WDS1H4	17.1	959.9	44.8	14.7	258.4	135.1	18.8	25.6	7.2	162.0	24.7	102.3	281.7	5.2	12.8	313.0	48.7	60.2	75.7
CYFS1H1	41.6	388.2	97.6	31.3	113.7	83.8	26.3	53.0	11.9	115.3	61.6	144.5	77.2	15.5	9.7	129.0	25.5	71.2	120.0
CYFS1H2	3.9	447.7	118.2	11.4	132.2	44.5	21.5	44.7	16.9	53.9	26.4	174.1	84.9	15.9	3.0	155.0	42.3	84.2	199.1
CYFS1H2i	2.5	460.2	131.9	12.0	109.0	45.6	21.3	78.7	17.1	52.4	30.8	163.5	81.2	15.1	4.1	127.2	41.7	69.2	210.3
CYFS1H3	35.9	363.1	101.5	36.0	113.1	87.2	25.6	45.3	12.3	112.2	54.7	145.9	78.0	15.3	10.1	137.5	25.1	52.2	123.9
CYFS1H4	29.4	358.0	123.3	7.1	117.6	19.4	23.6	53.7	12.7	21.0	73.8	163.9	80.7	13.3	6.7	129.7	25.6	27.7	126.8
RTS1H2	6.2	348.6	79.0	LOD	80.5	25.3	4.5	50.6	8.0	13.0	22.9	76.8	81.4	5.4	4.6	41.9	23.3	11.9	161.3
RTS1H3	5.8	545.6	84.9	5.1	86.4	33.5	7.7	49.4	9.5	10.9	30.7	98.5	116.2	8.0	6.1	59.8	50.3	13.4	184.2
RTS1H4	6.3	379.1	59.2	LOD	71.7	25.3	5.1	43.6	7.7	12.3	34.2	82.5	89.5	6.5	5.1	48.8	27.4	13.7	154.2
RTS1H5	7.2	226.9	59.7	LOD	72.7	24.0	1.0	36.9	3.9	3.6	38.8	40.5	120.0	4.1	5.9	61.8	21.6	10.1	144.8
RTS2H1	2.7	272.3	42.3	6.7	87.2	27.9	10.6	33.6	10.8	43.0	17.2	118.5	146.6	7.4	2.9	89.4	31.5	26.6	138.2
RTS2H2	6.9	282.9	55.3	7.9	77.4	62.1	7.0	42.9	8.0	50.3	25.3	92.2	48.7	5.7	3.6	135.8	34.6	22.6	113.1
RTS2H3	2.4	335.7	43.4	LOD	63.5	13.9	3.4	42.2	8.1	10.1	50.0	89.8	58.9	6.1	3.0	96.3	18.3	11.3	90.8
RTS2H4	8.6	507.7	55.0	6.4	105.9	26.5	12.3	43.7	12.9	55.2	19.3	138.5	78.8	6.3	3.6	81.9	25.4	42.9	162.7
RTS3H1	4.7	155.4	43.4	LOD	51.0	20.5	8.9	33.6	4.3	29.9	13.1	61.9	346.6	4.3	10.0	40.3	34.0	10.5	46.4
RTS5H1	5.8	323.9	52.1	LOD	80.2	10.6	5.6	32.7	8.0	15.3	18.5	85.8	77.1	5.7	3.4	48.6	20.2	9.2	162.0
RTS6H1	3.2	514.2	25.9	LOD	45.9	29.0	9.2	28.6	4.6	33.2	13.6	63.3	333.0	5.0	7.6	78.8	33.9	11.4	48.6
CVS1H1	9.3	295.9	66.8	10.3	87.8	26.2	10.1	35.9	10.1	38.2	18.0	100.8	67.0	8.0	2.4	54.7	30.8	16.5	195.8
CVS2H1	7.2	293.2	56.2	LOD	87.2	23.0	4.9	30.4	9.2	33.0	20.1	98.1	72.9	9.1	1.3	58.6	32.4	16.5	199.7
CVS3H1	7.2	273.8	55.3	LOD	91.2	21.5	7.4	36.6	10.1	28.0	14.7	95.8	68.9	7.6	2.4	63.4	34.4	17.8	260.9
CVS3H2	7.8	299.0	91.2	LOD	90.8	26.6	6.3	44.1	9.7	35.3	16.6	98.1	79.7	10.7	2.4	64.2	33.9	19.3	257.2

References:

Andrews, I.J., 2013, The Carboniferous Bowland Shale gas study: geology and resource estimation. *British Geological Survey for Department of Energy and Climate Change, London, UK*. URI: <http://nora.nerc.ac.uk/id/eprint/503839>

Armitage, P.J., Faulkner, D.R., Worden, R.H., Aplin, A.C., Butcher, A.R., Iliffe, J., 2011, Experimental measurement of, and controls on, permeability and permeability anisotropy of caprocks from the CO₂ storage project at the Krechba Field, Algeria, *Journal of Geophysical Research: Solid Earth*, **116**, B12208. DOI: 10.1029/2011JB008385

Armstrong, J.P., Smith, J., D'Elia, V.A.A., Trueblood, S.P., 1997, The occurrence and correlation of oils and Namurian source rocks in the Liverpool Bay- North Wales area, *Geological Society, London, Special Publications*, **124**, pp. 195-211. DOI: 10.1144/GSL.SP.1997.124.01.12

Arthurton, R.S., Johnson, E.W., Mundy, D.J.C., 1988, Geology of the country around Settle, *Memoir of the British Geological Survey*, Sheet 60 (England & Wales).

Bott, M.H.P., Johnson, G.A.L., 1967, The controlling mechanism of Carboniferous cyclic sedimentation, *Quarterly Journal of the Geological Society of London*, **122**, pp. 421-441. DOI: 10.1144/gsjgs.122.1.0421

Calvert, S.E., 2004, Beware intercepts: interpreting compositional ratios in multi-component sediments and sedimentary rocks, *Organic Geochemistry*, **35**, pp. 981-987. DOI: 10.1016/j.orggeochem.2004.03.001

Church, K.D., Gawthorpe, R.L., 1994, High resolution sequence stratigraphy of the late Namurian in the Widmerpool Gulf (East Midlands, UK), *Marine and Petroleum Geology*, **11**, pp. 528-544. DOI: 10.1016/0264-8172(94)90066-3

Collinson, J.D., 1988, Controls on Namurian sedimentation in the Central Province basins of northern England, in *Sedimentation in a Synorogenic Basin Complex: the Upper Carboniferous of Northwest Europe* (eds Besly B. M., Kelling G), Blackie, Glasgow, pp. 85–101, ISBN: 0216920256.

Davies, J.R., Wilson, D., Williamson, I.T., 2004, Geology of the Country around Flint, *Memoir for 1:50000 Geological Sheet 108 (England and Wales)*, British Geological Survey, ISBN: 085272487-X.

Davies, S.J., Hampson, G.J., Elliott, T., Flint, S.S., 1999, Continental-scale sequence stratigraphy of the Namurian, Upper Carboniferous and its applications to reservoir prediction, *Petroleum Geology of NW Europe: Proceedings of the 5th Conference*, edited by A. J. Fleet and S. A. R. Boldy, pp. 757–770, Geol. Soc., London. DOI: 10.1144/0050757

Davies, S.J., Leng, M.J., Macquaker, J.H.S., Hawkins, K., 2012, Sedimentary process control on carbon isotope composition of sedimentary organic matter in an ancient shallow-water shelf succession, *Geochemistry Geophysics Geosystems*, **13** (1), Q0AI04. DOI: 10.1029/2012GC004218

Dewhurst, D.N., Aplin, A.C., Sarda, J.P., Yang, Y.L., 1998, Compaction-driven evolution of porosity and permeability in natural mudstones: An experimental study, *Journal of Geophysical Research: Solid Earth*, **103** (B1), pp. 651-661. DOI: 10.1029/97JB02540

Espitalié, J., Laporte, J.L., Madec, M., Marquis, F., Leplat, P., Paulet, J., Boutefeu, A., 1977, Rapid method for source rock characterization, and for determination of their petroleum

potential and degree of evolution, *Oil & Gas Science and Technology - Revue de l'Institut Français du Pétrole*, **32** (1), pp. 23-42. DOI: 10.2516/ogst:1977002

Fraser, A.J., Gawthorpe, R.L., 1990, Tectono-stratigraphic development and hydrocarbon habitat of the Carboniferous in northern England, *Geological Society, London, Special Publications*, **55**, pp. 49-86. DOI: 10.1144/GSL.SP.1990.055.01.03

Fraser, A.J., Gawthorpe, R.L., 2003, An Atlas of Carboniferous Basin Evolution in Northern England, *Geological Society Memoirs*, **28**, 88 pages. ISBN: 1862391351

Gasparik, M., Ghanizadeh, A., Bertier, P., Gensterblum, Y., Bouw, S., Krooss, B.M., 2012, High-Pressure Methane Sorption Isotherms of Black Shales from The Netherlands, *Energy & Fuels*, **26** (8), pp. 4995-5004. DOI: 10.1021/ef300405g

Gross, D., Sachsenhofer, R.F., Bechtel, A., Pytlak, L., Rupprecht, B., Wegerer, E., 2015, Organic geochemistry of Mississippian shales (Bowland Shale Formation) in central Britain: Implications for depositional environment, source rock and gas shale potential, *Marine and Petroleum Geology*, **59**, pp. 1-21. DOI: <http://dx.doi.org/10.1016/j.marpetgeo.2014.07.022>

Guion, P.D., Fielding, C.R., 1988, Westphalian A and B sedimentation in the Pennine Basin, UK, in *Sedimentation in a Synorogenic Basin Complex: the Upper Carboniferous of Northwest Europe* (eds Besly B. M., Kelling G), Blackie, Glasgow, pp. 85–101, ISBN: 0216920256.

Hampson, G.J., Elliott, T., Flint, S.S., 1996, Critical application of high resolution sequence stratigraphic concepts to the Rough Rock Group (Upper Carboniferous) of northern England, *Geological Society, London, Special Publications*, **104**, p. 221-246. DOI: 10.1144/GSL.SP.1996.104.01.14

Hart, B.S., Macquaker, J.H.S., Taylor, K.G., 2013, Mudstone (“shale”) depositional and diagenetic processes: Implications for seismic analyses of source-rock reservoirs, *Interpretation (SEG)*, **1**(1), B7-B26. DOI: 10.1190/INT-2013-0003.1

Jarvie, D.M., Hill, R.J., Ruble, T.E., Pollastro, R.M., 2007, Unconventional shale-gas systems: The Mississippian Barnett Shale of north-central Texas as one model for thermogenic shale-gas assessment, *AAPG Bulletin*, **91** (4), pp. 475-499. DOI: 10.1306/12190606068

Jarvie, D.M., 2011, Unconventional Oil Petroleum Systems: Shales and Shale Hybrids, *AAPG Search and Discovery Article*, #80131.

Jerrett, R.M., Hampson, G.J., 2007, Sequence stratigraphy of the upper Millstone Grit (Yeadonian, Namurian), North Wales, *Geological Journal*, **42**, pp. 513-530. DOI: 10.1002/gj.1089

Johnson, E.W., Soper, N.J., Burgess, I.C., 2001, Geology of the country around Ulverston, *Memoir of the British Geological Survey*, Sheet 48 (England & Wales).

Jones, R.C.B., Lloyd, W., 1942, The stratigraphy of the Millstone Grit of Flintshire, *Journal of the Manchester Geological Association*, **13**, pp. 78-99.

Jones, B., Manning, D.A.C., 1994, Comparison of geochemical indexes used for the interpretation of palaeoredox conditions in ancient mudstones, *Chemical Geology*, **111** (1-4), pp. 111-129. DOI: 10.1016/0009-2541(94)90085-X

Junium, C.K., Arthur, M.A., 2007, Nitrogen cycling during the Cretaceous, Cenomanian–Turonian Oceanic Anoxic Event II, *Geochemistry, Geophysics, Geosystems*, **8** (3), Q03002. DOI: 10.1029/2006GC001328.

- Lewan, M.D., 1986, Stable carbon isotopes of amorphous kerogens from Phanerozoic sedimentary-rocks, *Geochimica et Cosmochimica Acta*, **50** (8), pp. 1583-1591. DOI: 10.1016/0016-7037(86)90121-3
- Martinsen, O.J., Collinson, J.D., Holdsworth, B.K., 1995, Millstone Grit cyclicity revisited, II: sequence stratigraphy and sedimentary responses to changes of relative sea-level, *Sedimentary Facies Analysis: A Tribute to the Research and Teaching of Harold G. Reading (ed A. G. Plint)*, Blackwell Publishing Ltd., Oxford, UK. DOI: 10.1002/9781444304091.ch13
- Meyers, P.A., Bernasconi, S.M., Yum, J-G., 2009, 20 My of nitrogen fixation during deposition of mid-Cretaceous black shales on the Demerara Rise, equatorial Atlantic Ocean, *Organic Geochemistry*, **40** (2), pp. 158-166. DOI: 10.1016/j.orggeochem.2008.11.006
- Milliken, K.L., Esch, W.L., Reed, R.M., Zhang, T.W., 2012, Grain assemblages and strong diagenetic overprinting in siliceous mudrocks, Barnett Shale (Mississippian), Fort Worth Basin, Texas, *AAPG Bulletin*, **96** (8), pp. 1553-1578. DOI: 10.1306/12011111129
- Montgomery, S.L., Jarvie, D.M., Bowker, K.A., Pollastro, R.M., 2005, Mississippian Barnett Shale, Fort Worth basin, north-central Texas: Gas-shale play with multi-trillion cubic foot potential, *AAPG Bulletin*, **89** (2), pp. 155-175. DOI: 10.1306/09170404042
- Passey, Q. R., Bohacs, K. M., Esch, W. L., Klimentidis, R., Sinha, S., 2010, From oil-prone source rock to gas-producing shale reservoir: Geologic and petrophysical characterization of unconventional shale-gas reservoirs: International Oil and Gas Conference and Exhibition in China, Beijing, China, June 8–10, 2010, SPE Paper 131350, 29 p.
- Peters-Kottig, W., Strauss, H., Kerp, H., 2006, The land plant $\delta^{13}\text{C}$ record and plant evolution in the Late Palaeozoic, *Palaeogeography Palaeoclimatology Palaeoecology*, **240** (1-2), pp. 237-252. DOI: 10.1016/j.palaeo.2006.03.051

Ramsbottom, W.H.C., 1974, The Namurian of North Wales, in Owen, T.R., *The Upper Palaeozoic and post-Palaeozoic of North Wales*, Cardiff University Press, 426 pages, ISBN: 0-7083-0555-5.

Ramsbottom, W.H.C., 1977, Major cycles of transgression and regression (mesothems) in the Namurian, *Proceedings of the Yorkshire Geological Society*, **41**, pp. 261-291.

Ramsbottom, W.H.C., 1978, Namurian mesothems in South Wales and northern France, *Journal of the Geological Society*, **135**, pp. 307-312. DOI: 10.1144/gsjgs.135.3.0307

Rexer, T.F.T., Benham, M.J., Aplin, A.C., Thomas, K.M., 2013, Methane Adsorption on Shale under Simulated Geological Temperature and Pressure Conditions, *Energy & Fuels*, **27** (6), pp. 3099-3109. DOI: 10.1021/ef400381v

Rivera, K., Quan, T. M., 2013, Thermal maturation effects on the nitrogen isotopes in marine shales: a case study of the Woodford Shale, *AAPG Annual Convention and Exhibition*. Abstract published as Search and Discovery article #50920 (2014).

Rose, W.C.C., Dunham, K.C., 1977, Geology and hematite deposits of South Cumbria, *Economic Memoir of the British Geological Survey*, Sheet 58, Part 48.

Ross, D.J.K., Bustin, R.M., 2009, Investigating the use of sedimentary geochemical proxies for paleoenvironmental interpretation of thermally mature organic-rich strata: Examples from the Devonian-Mississippian shales, Western Canadian Sedimentary Basin, *Chemical Geology*, **260**, pp. 1-19. DOI: 10.1016/j.chemgeo.2008.10.027

Rygel, M.C., Fielding, C.R., Frank, T.D., Birgenheier, L.P., 2008, The magnitude of late Palaeozoic glacioeustatic fluctuations: a synthesis, *Journal of Sedimentary Research*, **78** (7-8), pp. 500-511. DOI: 10.2110/jsr.2008.058

Stephenson, M.H., Millward, D., Leng, M.J., Vane, C.H., 2008, Palaeoecological and possible evolutionary effects of early Namurian (Serpukhovian, Carboniferous) glacioeustatic cyclicality, *Journal of the Geological Society, London*, **165**, pp. 993-1005. DOI: 10.1144/0016-76492007-153

Schieber, J., Krinsley, D., Riciputi, L., 2000, Diagenetic origin of quartz silt in mudstones and implications for silica cycling, *Nature*, **406**, p. 981-985. DOI: 10.1038/35023143

Schieber, J., Southard, J.B., Thaisen, K., 2007, Accretion of Mudstone Beds from Migrating Floccule Ripples, *Science*, **318**, p. 1760-1763. DOI: 10.1126/science.1147001

Schieber, J., Southard, J.B., Schimmelmann, A., 2010, Lenticular Shale Fabrics Resulting from Intermittent Erosion of Muddy Sediments – Comparing Observations from Flume Experiments to the Rock Record, *Journal of Sedimentary Research*, **80**, p. 119-128. DOI: 10.2110/jsr.2010.005

Słowakiewicz M., Tucker, M.E., Vane, C.H., Harding, R., Collins, A., Pancost, R.D., 2015, Shale-Gas Potential of the Mid-Carboniferous Bowland-Hodder Unit in the Cleveland Basin (Yorkshire), Central Britain, *Journal of Petroleum Geology*, **38**(1), pp.59-76. DOI: 10.1111/jpg.12598

Tissot, B.P., Welte, D.H., 1984, Petroleum Formation and Occurrence: a new approach to oil and gas exploration [2nd Edition], *Springer-Verlag, New York*, pp.538, ISBN 978-3642878152

Tyson, R.V., Follows, B., 2000, Palynofacies prediction of distance from sediment source: A case study from the Upper Cretaceous of the Pyrenees, *Geology*, **28** (6), pp. 569-571. DOI: 10.1130/0091-7613(2000)28<569:PPODFS>2.0.CO;2

Van Mooy, B.A.S., Keil, R.G., Devol, A.H., 2002, Impact of suboxia on sinking particulate organic carbon: enhanced carbon flux and preferential degradation of amino acids via

denitrification, *Geochimica et Cosmochimica Acta*, **66** (3), pp.457–465. DOI: 10.1016/S0016-7037(01)00787-6

Verardo, D.J., MacIntyre, A., 1994, Production and destruction: control of biogenous sedimentation in the tropical Atlantic 0–300,000 years B.P., *Paleoceanography*, **9** (1), pp.63–86. DOI: 10.1029/93PA02901

Waters, C.N., Waters, R.A., Barclay, W.J., Davies, J.R., 2009, A lithostratigraphical framework for the Carboniferous successions of southern Great Britain (Onshore), *British Geological Survey Research*, Report RR/09/01.

Waters, C.N., 2009, Carboniferous geology of Northern England, *Journal Open University Geological Society*, **30** (2), pp. 5-16. URI: <http://nora.nerc.ac.uk/id/eprint/10713>

Waters, C.N., Condon, D.J., 2012, Nature and timing of Late Mississippian to Mid-Pennsylvanian glacio-eustatic sea-level changes of the Pennine Basin, UK, *Journal of the Geological Society*, **169** (1), pp. 37-51. DOI: 10.1144/0016-76492011-047

Wedepohl, K.H., 1971, Environmental influences on the chemical composition of shales and clays. In: Ahrens, L.H., Press, F., Runcorn, S.K., Urey, H.C. (Eds.), *Physics and Chemistry of the Earth*, vol. **8**, Pergamon, Oxford, pp. 305–333.

Wells, M.R., Allison, P.A., Hampson, G.J., Piggott, M.D., Pain, C.C., 2005, Modelling ancient tides: the Upper Carboniferous epi-continental seaway of Northwest Europe, *Sedimentology*, **52** (4), pp. 715-735. DOI: 10.1111/j.1365-3091.2005.00718.x

Williams, G.D., Eaton, G.P., 1993, Stratigraphic and structural analysis of the Late Palaeozoic-Mesozoic of NE Wales and Liverpool Bay: implications for hydrocarbon prospectivity, *Journal of the Geological Society*, **150** (3), pp. 489-499. DOI: 10.1144/gsjgs.150.3.0489

Wright, W.B., Sherlock, R.L., Wray, D.A., Lloyd, W., Tonks, L.H., 1927, Geology of the Rossendale Anticline, *Memoir of the Geological Survey of Great Britain*, Sheet 76 (England & Wales).

Yang, Y.L., Aplin, A.C., 2007, Permeability and petrophysical properties of 30 natural mudstones, *Journal of Geophysical Research: Solid Earth*, **112** (B3), B03206. DOI: 10.1029/2005JB004243

Yang, Y.L., Aplin, A.C., 2010, A permeability-porosity relationship for mudstones, *Marine and Petroleum Geology*, **27** (8), pp. 1692-1697. DOI: 10.1016/j.marpetgeo.2009.07.001